Permanganate-Based Synthesis of Semiconducting Metal Oxide Nanoparticles in the Protein Ferritin

Cameron Olsen

A senior thesis submitted to the faculty of
Brigham Young University
in partial fulfillment of the requirements for the degree of

Bachelor of Science

John Colton, Advisor

Department of Physics and Astronomy

Brigham Young University

April 2016

ABSTRACT

Permanganate-Based Synthesis of Semiconducting Metal Oxide Nanoparticles
in the Protein Ferritin

Cameron Olsen
Department of Physics and Astronomy, BYU
Bachelor of Science

This thesis investigates the reactions of Mn^{2+} and Co^{2+} with permanganate as a route for manganese and cobalt oxide nanoparticle synthesis in the protein ferritin. Permanganate serves as the electron acceptor and reacts with Mn^{2+} and Co^{2+} in the presence of apoferritin to form manganese and cobalt oxide cores inside the protein shell. Manganese loading into ferritin was studied under acidic, neutral, and basic conditions and the ratios of Mn^{2+} and permanganate were varied at each pH, while cobalt loading was studied at pH 8.5 only. The manganese and cobalt-containing ferritin samples were characterized by transmission electron microscopy, UV/Vis absorption, and by measuring the band gap energies for each sample. Manganese cores formed in both the acidic and basic conditions, while a mixed cobalt-manganese core formed at the desire pH. New manganese oxide cores formed in the acidic manganese trials and have absorption profiles and band gap energies that are different from the Mn(O)OH cores synthesized by the traditional method of using oxygen. These new manganese cores have indirect band-gap transitions ranging from 1.63 to 1.68 eV, which differ from the band gap energy of 1.53 eV for Mn(O)OH ferritin. In addition, an increased absorption around 370 nm was observed for the new manganese cores, suggestive of MnO_2 formation inside ferritin. The mixed cobalt-manganese samples showed band gaps ranging from 1.48 eV up to 1.75 eV, which correlated with the final ratio of cobalt and manganese present in the material.

Keywords: Ferritin, Manganese, Cobalt, Synthesis, Permanganate, Comproportionation

ACKNOWLEDGMENTS

This work has been possible through the help and support of many people, and I am grateful for each of their contributions. I start off by thanking and acknowledging my advisor Dr. John Colton as he has helped guide me in my research, providing counsel, direction, and feedback at each stage of the research process, as well as for his friendship and valued advice. I also wish to thank Dr. Richard Watt for his support and assistance as I worked alongside him in his lab. I thank my fellow students for helping me with all stages of research, which students include Jacob Embley, Trevor Smith, Stephen Erickson, Alessandro Perego, Kameron Hansen, Ryan Peterson, Andrew Henrichson, and Jake Maxfield. I also wish to express thanks to Michael Meehan for his humor and friendship during research and classes. I thank the Utah Office of Energy Development and the BYU Department of Physical and Mathematical Sciences for providing the funding necessary to carry out this research. Lastly, I thank my wife Rachel for her unending support as I've worked towards my dreams.

Contents

List of Figures

List of Tables

Chapter 1

Introduction

1.1 Overview of Thesis

Energy production is a major concern for modern society. Difficulties lie in finding a renewable and efficient means to produce clean and sustainable energy. The majority of the global economy is fueled by fossil fuels, which are both nonrenewable and harmful to the environment. Due to the environmental impact and limited nature of fossil fuels, researchers and governments worldwide are seeking new ways to harvest energy.

The protein ferritin has been studied for over half a century. While many things are known about ferritin, there are still areas that are not well understood. Its ability to store iron in the blood as a ferrihydrite nanoparticle endows it with unintended properties, including its potential to act as a semiconducting material. By replacing the iron interior with other transition metals, we are able to change the band gap energy of the ferritin nanoparticle. Ferritin is thus able to operate as a substrate for solar energy absorption with possible applications in fuel cell technologies.

My goal is to expand the current minerals available inside of ferritin to increase the efficiency of solar energy absorption. The metals inside of ferritin are some of the most common transition

metals found in the earth, and this combined with the organic nature of the protein leads to an environmentally friendly and cheap way to capture solar energy.

By using the molecule permanganate I will study new minerals inside of ferritin. This thesis will follow the introduction, synthesis, and analysis of these ferritin minerals, and discuss their applicability in absorbing light from the solar spectrum.

1.2 The Protein Ferritin

Ferritin is a protein found in many living organisms. The protein is composed of 24 subunits arranged into a sphere, which collectively weigh approximately 450 kDa [1,2]. The sphere measures 12 nm in diameter, with an 8 nm diameter hollow interior. Two different subunits called the light chain and the heavy chain make up the protein shell. Their names refer to the relative molecular weight of each subunit, and they are cited in literature as the L-chain and H-chain, respecitvely. Either chain can be used independently to form ferritin, though each chain is used for different purposes [3,4]. The H-chain is responsible for the ferroxidase activity of ferritin (meaning the oxidation of iron), while the L-chain is home to nucleation sites for iron mineral growth [3]. The site for iron oxidation in the H-chain is called the ferroxidase center. The specific amino acid residues inside the H-chain bind the iron and facilitate their oxidation by oxygen. The structure of ferritin enables it to withstand temperatures up to 70°C and a pH range varying from 3.4-10 [5–7]. Though the ferritin shell remains intact for a pH value as low as 3.4, the protein will precipitate around its isoelectric point (pI) at pH 4.4 [8–10], which can be reversed by again raising the pH.

Ferritin's primary role in nature is to store excess iron as a ferrihydrite mineral [Fe(O)OH] and act as a buffering system throughout the body. Iron enters through the channels formed between the individual subunits and makes its way to the H-chain ferroxidase center. Each ferroxidase center can hold two iron atoms. Oxygen then oxidizes both iron atoms from their Fe^{2+} state to Fe^{3+} ions

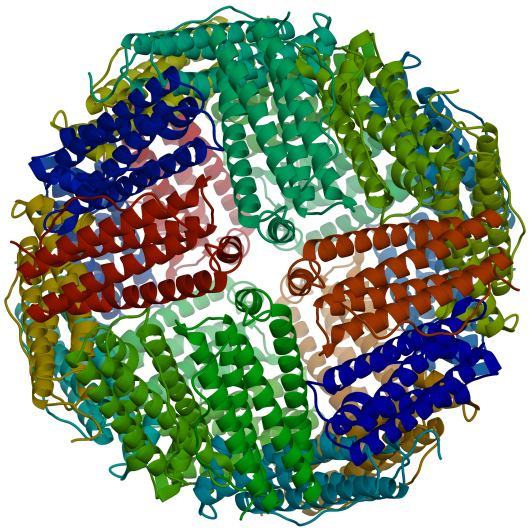

Figure 1.1 The protein ferritin is a spherical protein consisting of 24 subunits. Model generated using UCSF Chimera software package, PDB code 1FHA.

inside of the protein shell. The Fe^{3+} ions migrate to the L-chain where the ferrihydrite mineral forms. Once a mineral has begun forming, the iron will deposit on the surface of the mineral itself. The inside of ferritin can load up to 4500 iron atoms, giving ferritin a great capacity for iron uptake in the blood [4,5]. Lastly, oxygen is converted into hydrogen peroxide upon acceptance of the two electrons.

In addition to the oxidation of lower-oxidation state transition metals, ferritin also has the capacity to incorporate oxoanions such as phosphate into its interior [11–14]. Their addition affects both the loading and the properties of the mineral core [15].

1.3 Non-Native Nanoparticles in Ferritin

Removing the native iron core makes room for incorporating other transition metals into ferritin. Dialyzing the ferritin against thioglycolic acid removes the ferrihydrite mineral, and the resulting ferritin shell is termed apoferritin. The thioglycolic acid chelates the iron, meaning it pulls it away

from the core and binds it, and the resulting Fe(III)-thiolate complex causes the solution to turn purple.

Once apoferritin has been formed and isolated, non-native transition metals can be inserted into the core by two methods. The first of these methods involves the gradual deposition of the mineral into the apoferritin shell. This often occurs through the use of the ferroxidase center, though it does not preclude the possibility that the core could form independently inside the shell. Similar to the ferrihydrite production, molecular oxygen is used as the standard electron acceptor, though hydrogen peroxide can be used in situations where oxygen is insufficeint [7].

A second, though less utilized method, involves the disassembly and reassembly of the ferritin subunits [16]. The nanoparticle cores are formed independently of ferritin, and the ferritins are dissassembled by lowering the pH of the solution. Reassembly occurs upon increasing the pH of the solution, and some of the ferritins will form around the nanoparticle cores themselves. Though this is a viable route for nanoparticle synthesis, it is generally not the preferred method for inserting cores into ferritin as incomplete protein formation may occur [5].

Many non-native nanoparticles have been formed inside of ferritin, including Co(O)OH, Mn(O)OH, Ti(O)OH, PbS, FeS, CdS, and noble metal nanoparticles [16–23]. The majority of these nanoparticles have been formed through the first method of mineral deposition inside ferritin.

Smith et al. recently observed that using permanganate results in the formation of an iron-manganese core inside of ferritin [15]. This discovery indicates a new possible route for the incorporation of metals into apoferritin. As stated above, the use of oxygen or peroxide has been the typical approach for the oxidation of the lower transition state metals (typically a 2+ state). However, the observation by Smith et al. suggests that permanganate is able to replace oxygen as the electron acceptor and simultaneously be incorporated into the ferritin core.

Using a similar technique we can also observe a bimetal, or mixed metal, oxy-hydroxide core in ferritin. Literature has shown how ferritin can load a bimetal core consisting of iron and manganese

[24]. However, this was done follwing standard sythesis procedures with iron and manganese as electron donors in the 2+ state, while this new method would use manganese in a high, 7+ oxidation state.

These results led me to synthesize a new manganese oxide nanoparticle inside of ferritin using permanganate. Additionally, I used permanganate to create a new bimetal core consiting of cobalt and manganese in the protein ferritin.

1.4 Permanganate as the Oxidant for Nanoparticle Synthesis

Permanganate is a polyatmoic anion consisting of one manganese metal bound to four oxygen atoms, written as MnO_4^- (see Fig. 1.2). The manganese ion is a semi-stable cation in the 7+ oxidation state, and if dissolved in water turns the solution a deep, vibrant purple color. Due to the high positive charge on the manganese atom, permanganate is a strong oxidizing agent, meaning it is able to take or accept electrons from a wide host of molecules. As permanganate is reduced, or receives electrons, the oxidation state of the metal decreases and it is able to form new manganese minerals. Manganese is relatively stable in the 2+, 3+, and 4+ states. Mn^{2+} is generally quite soluble in water, while Mn^{3+} and Mn^{4+} are more likely to form insoluble compounds with oxygen [25]. Mn^{4+}predominantly forms MnO_2, which is completely insoluble in water, though under reducing conditions it can accept electrons and form Mn^{2+} [26].

Since manganese can be in multiple oxidation states, it can undergo what is termed a comproportionation reaction. In this reaction, there are two separate manganese reactants, one at a high oxidation state and one at a lower oxidation state. With the right amount of each reagent, the reaction can result in a single manganese compound with one oxidation state. One such comproportionation reaction,

$$3\,Mn^{2+} + 2\,MnO_4^- + 2\,H_2O \rightarrow 5\,MnO_2 + 4\,H^+, \tag{1.1}$$

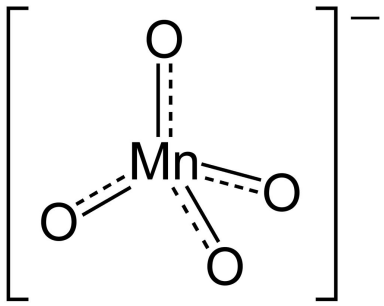

Figure 1.2 The molecule permanganate consists of a central manganese ion surrounded by four oxygen molecules.

results in the formation of a single Mn^{4+} compound. As shown in Eq. 1.1, this reaction forms a single manganese compound with one oxidation state from two separate manganese ions with different oxidation states.

The reaction of permanganate with either Mn^{2+} or Co^{2+} has the potential to undergo two reactions to incorporate itself into the interior of ferritin. The first pathway involves the ferroxidase center in ferritin. As is the case for its natural substrate iron, the ferroxidase center binds two divalent ions, where they await oxidation. Rather than oxygen, permanganate accepts the electrons and allows the trivalent metal to be incorporated into the metal core. After accepting two electrons, permanganate results in a Mn^{5+} species. This Mn^{5+} either recycles to accept two more electrons and form a Mn^{3+} compound, namely Mn(O)OH, as shown in Eq. 1.2, or is too unstable to be recycled and reacts by other pathways [25]. These reactions are purposefully left unbalanced because the reactions are performed under acidic, neutral, and basic conditions, which alters the stoichiometry of the equations. These equations are outlined below as

$$\text{Apoferritin} + 4\,Mn^{2+} + MnO_4^- \rightarrow 5\,Mn(O)OH \tag{1.2}$$

$$\text{Apoferritin} + 2\,Mn^{2+} + MnO_4^- \rightarrow 2\,Mn(O)OH + Mn^{5+}. \tag{1.3}$$

Note that divalent manganese can be replaced with cobalt, which is similarly incorporated into the ferritin core as the oxyhydroxide Co(O)OH [7].

The second pathway involves the direct reaction of the metal ion and permanganate inside of ferritin. As previously stated, oxoanions like permanganate have the ability to diffuse into ferritin. Divalent metal atoms also can diffuse into the ferritin cavity [27–31]. Once these have diffused into the interior, they react and form metal oxide nanoparticles inside of ferritin, using the shell as a template for mineralization rather than a catalyst. Following is a comproportionation reaction where the final mineral is a 4^+ state (see Eq. 1.4). Though Eq. 1.4 is the most likely reaction, the comproportionation of Mn^{2+} and permanganate could also potentially form a Mn^{3+} mineral. Such a reaction could similarly be represented by Eq. 1.2. Note that cobalt cannot be oxidized by permanganate past the Co^{3+} state and will not follow Eq. 1.4. The partial equation for the formation of Mn^{4+} is as follows:

$$\text{Apoferritin} + 3\,Mn^{2+} + 2\,MnO_4^- \rightarrow 5\,MnO_2. \tag{1.4}$$

As stated above, Co^{2+} is not a viable option for Eq. 1.4, where the result is a metal in a positive four oxidation state; it can only follow the reaction listed in Eqs. 1.2 or 1.3. The result of the direct comproportionation of manganese inside of ferritin also has the potential to form another Mn^{3+} compound, Mn_2O_3, though it is undetermined which mineral type will form preferentially.

We chose to use the ratios between Mn^{2+} and MnO_4^- outlined in Equations 1.2–1.4 as a basis for our synthesis methods. By varying the ratio between these reactants we hoped to control the pathway by which their reaction occured. However, we acknowledge that these two pathways do not necessarily act independently, and likely act concurrently to produce cores inside of ferritin. Since permanganate can be present both inside and outside the ferritin shell it has the potential to undertake both roles when reacting with either Mn^{2+} or Co^{2+}. These two pathways for manganese are shown in Figure 1.3.

Permanganate is also known to target certain amino acids in proteins (tyrosine and tryptophan, both common in ferritin) and cleave the protein into pieces [32]. We also recognized that permanganate might similarly oxidize and denature ferritin in the absence of an electron rich molecule,

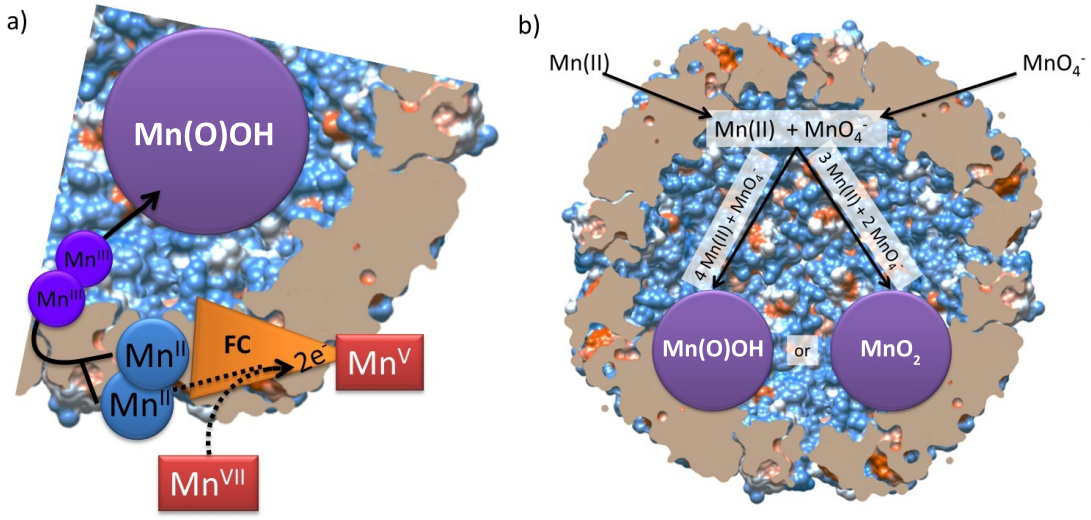

Figure 1.3 (a) The ferroxidase center pathway. Mn^{2+} binds at the ferroxidase center (FC) and is oxidized to Mn^{3+} by permanganate. After oxidation the Mn^{3+} ions migrate to the ferritin interior and become mineralized as a Mn^{3+} compound. This pathway follows the reactions given in Eqs. 1.2 and 1.3. (b) The comproportionation pathways. Manganese and permanganate first enter ferritin and then react to form either a Mn^{3+} or Mn^{4+} mineral. This diagram follows Eqs. 1.2 and 1.4, which are represented the left-hand and right-hand pathways in the figure, respectively.

i.e., causes the unfolding of the protein, resulting in loss of structure and function.

I report the successful synthesis of two different nanoparticles inside of ferritin while using permanganate. The first of these is a manganese oxide mineral, while the latter is a bimetal core consiting of both cobalt and manganese oxides.

1.5 Semiconducting Nature of Nanoparticles in Ferritin

Many ferritin minerals are semiconducting materials and can act as a substrate for light absorption. Most of the ferritin minerals are indirect transition materials, meaning they have an indirect band gap energy while also having a direct transition available [33]. As photosensitive materials are struck by energetic photons, the valence band electrons can be excited into a higher state. If

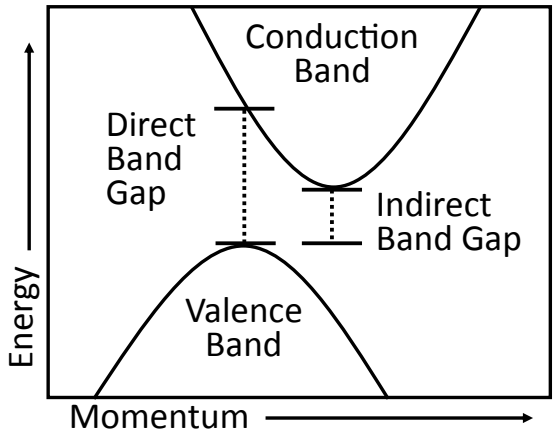

Figure 1.4 The general band structure of indirect band gap materials. Indirect band gap materials have both a direct and an indirect band gap. Electron excitation in indirect materials requires additional momentum obtained through phonon absorption.

the energy exceeds the band gap energy, electrons will be excited from the valence band into the conduction band and flow out of the material, ready to do work. Energy in excess of the band gap will dissipate as heat, and the electron will keep only the energy necessary to overcome the energy barrier. However, if the energy of the photon is less than the band gap energy, the photon will not be absorbed by the material and pass right through. Direct band gap materials need only a photon with enough energy to overcome the band gap. Indirect materials need both a high energy, low momentum photon and a low energy, high momentum phonon to cause electron excitation (a phonon is essentially a quantized vibration in the crystal lattice of the semiconductor), as demonstrated in Fig. 1.4.

The band gap energies for the common metal hydroxide minerals, e.g., Fe(O)OH, Mn(O)OH, Co(O)OH, and Ti(O)OH, correspond with wavelengths that lie in the visible section of the solar spectrum, making them ideal substrates for light harvesting [34]. Band gap energies can be accurately measured by optical absorption spectroscopy (OAS) [33].The reported values for the indirect and direct band gap energies for each metal core are: Mn(III)-ferritin, 1.60 eV and 2.83 eV; Co(III)-ferritin, 1.93 eV and 2.65 eV; Fe(III)-ferritin2.14 eV and 3.05 eV; and Ti(IV)-ferritin,

2.19 eV and 3.8 eV [33, 34]. By layering these materials in a multi-junction solar cell, it is possible to increase the efficiency of solar energy absorption as each layer absorbs only those photons which it converts most efficiently.

My two newly synthesized cores are semiconductors and have measurable band gap energies. Their addition to the current list of substrates increases the potential efficiency of our solar cells.

Chapter 2

Experimental Methods

2.1 Apoferritin Preparation

Before new metal oxide cores can be synthesized into ferritin, the native ferrihydrite mineral must be removed from inside ferritin. This is accomplished through dialysis. Native ferritin is placed inside a semi-permeable membrane with a cut-off value that is well below the molecular weight of ferritin (c. 450 kDa). Dialysis cassettes are preferred over using a dialysis membrane as the cassettes retain a greater percentage of the protein. Using dialysis materials allows the protein to remain inside while salts and smaller molecules can be freely exchanged across the membrane.

We used a 7000 molecular weight cut off 0.5-3.0 mL dialysis cassette from Cole-Parmer. The cassette was hydrated for several minutes in distilled water before the ferritin was inserted into the membrane. Hydrating the membrane ensures the integrity of the membrane and prevents the needle from puncturing the sides. Up to 3 mL of ferritin was inserted into the hydrated cassette and allowed to dialyze against a 5% thioglycolic acid 1 L solution buffered with 0.25 M sodium acetate at pH 4.8–5.0. The solution was stirred genlty for 8 hours and this procedure was repeated two more times. The thioglycolic acid enters the ferritin shell and complexes the iron, allowing it

to be dissolved into solution. The formation of the iron-thiol complex gives the solution a distinct medium-purple color. After three rounds of dialysis effectively all the iron is removed from the shell. A fourth round of dialysis is often helpful for some batches of ferritin that remain dark even after three rounds. By this point all iron will be removed except two iron atoms which are tightly bound to each ferroxidase center. If desired, these tightly bound iron atoms can be removed using a saturated bipyridine solution. However, for the purposes of our experiments they were ignored. The apoferritin-containing cassette is removed from the solution and added to a 0.5% bicarbonate solution and stirred for 8 hours. This is likewise repeated two more times. This last step removes the acid and old buffer from the cassette and replaces it with a neutral and weakly buffered solution. Once complete, the apoferritin is ready for nanoparticle synthesis.

2.2 Synthesis of Nanoparticles

Listed below are the synthesis methods for the manganese comproportionation samples and the cobalt/manganese mixed metal samples. The synthesis techniques were similar in almost every way except which divalent salt was used and the pH of the reaction buffer. Following the specifics for the synthesis of each sample, all remaining experimental sections apply to both types of samples.

2.2.1 Manganese Nanoparticle Synthesis

As stated in the introduction, the reaction of manganese is dependent upon the pH of the solution. Hence, three buffered solutions were used to test manganese comproportionation at different pH values. These buffers are as follows: 1 M pH 5.4 2-(N-morpholino)ethanesulfonic acid (MES), 1 M pH 7.4 imidazole, and 1 M pH 9.4 N-(1,1-Dimethyl-2-hydroxyethyl)-3-amino-2-hydroxypropanesulfonic acid (AMPSO). Each synthesis included 1 mL of one of these buffers, to

which 3.0 mg of apoferritin was added.

For the manganese comproportionation samples, $MnCl_2 \cdot 4H_2O$ and $KMnO_4$ were added to the buffered apoferritin solution to synthesize the manganese ferritin cores. Following the proposed equations in the introduction (Eqs. 1.2–1.4), the reagents were added in the following ratios of Mn^{2+} to MnO_4^-: 4 to 1, 2 to 1, and 3 to 2. (For the remainder of this thesis, each sample will be referred to by its ratio between Mn^{2+} and MnO_4^-.) As my purpose was to determine the effectiveness of permanganate as the electron acceptor, every synthesis was performed both aerobically and anaerobically. Each salt was prepared at 66.7 mM, and the appropriate volume of each reagent was added to the solution to achieve 150 metals/ferritin/injection. This was repeated for a total of 10 times, giving us 1500 Mn/ferritin. For example, in the 2:1 synthesis, 10 μL of 66.7 mM $MnCl_2$ and 5 μL of 66.7 $KmNo_4$ were added each round of injections. We waited 10 minutes between additions to allow time for the manganese to be incorporated into ferritin. This ratio was initially tested at all pH values, and it was observed that cores formed in the pH 5.4 and 9.4 solutions, but nothing formed in the 7.4 solution. Accordingly, we performed all the proposed ratios in both of the pH 5.4 and 9.4 solutions while choosing to exclude reactions at pH 7.4. Samples prepared using a ratio of Mn^{2+} and MnO_4^- are termed the *comproportionation* samples due to their proposed reaction mechanisms. In addition to the ratios above, I also ran control reactions with either entirely Mn^{2+} or entirely MnO_4^- to observe the effect each one had individually on core formation. Samples using permanganate only are termed the *permanganate only* reactions, while the samples using only Mn^{2+} are based off of the synthesis discovered by Meldrum et al. [6], which use oxygen instead of permanganate, and are termed the *traditional method*. These two reactions also targeted 1500 metals per ferritin.

2.2.2 Cobalt-Manganese Nanoparticle Synthesis

For the cobalt/manganese mixed metal samples, $Co(NO_3)_2$ and $KMnO_4$ were added to a pH 8.5 AMPSO buffer, following the conditions outlined in the Douglas et al. paper for the cobalt nanoparticle synthesis [7]. Different ratios ranging from 1600 Co/ferritin and 0 Mn/ferritin to 0 Co/ferritin and 1600 Mn/ferritin were targeted, with a total metal count being held constant at 1600 metals/ferritin. A total of 9 samples were run, with the number of metals per ferritin either increasing or decreasing by 200 each time (see Table 3.2). Both salts were prepared at a concentration of 53.3 mM, allowing for us to achieve 160 metals/ferritin/injection. A total of 10 injections were given, with 10 minutes between each injection. Due to the fact that oxygen is insufficient to oxidize cobalt from its 2+ state to its 3+ state, the effect of oxygen was negligible and all samples were run aerobically.

2.3 Protein Separation

After synthesis, the samples were centrifuged at $3100 \times g$ for 10 minutes, and the ferritin containing solution was decanted. The protein was separated from salts remaining in solution by passing each sample over a 15 cm $\times$ 1 cm Sephadex G-100 size exclusion column buffered with 25 mM pH 8.5 Tris, no salt. The cut-off value was chosen to ensure that the protein bypassed the matrix and the salts were separated. As is common with size exclusion columns, the molecules larger than the cut-off value eluted from the column first. The eluent was collected in 1 mL fractions until 24 mL total had been collected. The ferritin and its core eluted around the 5th and 6th fraction while the salt peaked around the 15th fraction.

Running the samples over the column separated the protein from any excess salts in solution. The absorbance was measured of each fraction at 255 nm, 280 nm, and 330 nm. Protein naturally absorbs light at 280 nm, though the presence of the ferritin core and remaining salts will also

increase that absorbance.

2.4 Protein Quantification

Once the protein has been isolated, we measured the protein concentration of each sample. Traditionally, the Lowry protein assay [35] is preferred for determining the concentration of ferritin. This is because the process denatures the protein and exposes all of its sidechains to the reagents, allowing for an accurate and consistent amount of amino acids in the sequence to be detected. However, the metals released from the core of our samples were found to interfere with the Lowry reagent and prevented an accurate determination of protein concentration. Because of this, we used the Bradford protein assay [36]. This method is generally less reliable for ferritin because the spherical shape prevents full interaction with the Bradford reagent. To account for this, a control apoferritin solution was used and the concentration was determined by measuring the 280 nm absorbance. Apoferritin has a known extinction coeffecient of 471,000 $cm^{-1}M^{-1}$ [37], from which the concentration can be calculated according to the Beer-Lambert law

$$A = \varepsilon cl, \tag{2.1}$$

where A is the absorbance, ε is the molar extinction coefficient, c is the concentration, and l is the path length that the light travels through. The concentration found using the 280 nm absorbance was then compared to the concentration found using the Bradford reagent, and the ratio between these two was used to correct the concentrations of ferritin samples measured using the Bradford assay. The Beer-Lambert law cannot be used for our ferritin samples as their cores also absorb 280 nm light and would alter the calculated concentration.

2.5 Metal Analysis

Metal analysis was performed by use of an inductively coupled plasma mass spectrometer (ICP-MS). Either 20 μL or 30 μL of each sample was injected into enough trace-metal grade 2% HNO_3 to form a 5 mL solution. These remained in solution overnight to allow for the breakdown of the ferritin shell and the dissolution of the metal cores. The samples were then centrifuged and ran through 0.2 um filters to remove any protein components from the solution. Standards were prepared at 0 ppb, 50 ppb, 100 ppb, 150 ppb, 200 ppb, and 1000 ppb of manganese and cobalt. These samples were taken to the ICP-MS and the metal concentrations were measured. These concentrations were used in conjunction with the protein concentration to calculate the average number of metals per ferritin, which is indicative of mineral size.

2.6 Imaging on the Transmission Electron Microscope

Samples were then prepared for imaging on a Technai TFf-20 Transmission Electron Microscope (TEM). Carbon 3 mm type-b 300 mesh copper grids from Ted Pella were placed under low vacuum. A high voltage was passed over the chamber, electrostatically charging the copper grids. Once the grids had been charged for at least 30 seconds, they were removed from the chamber and 3.5 μL of each sample was placed on the grids and allowed to sit for 1 minute before the excess solution was wicked away. The grids were rinsed in a drop of distilled water for 3 seconds. A uranyl acetate stain was used to help visualize the protein, and 3.5 μL of the uranly acetate solution was placed on each grid for 1 minute before it was wicked away and rinsed in distilled water.

Each sample was then viewed under the TEM and brightfield images were taken. The microscope was then turned to scanning transmission electron microscope (STEM) mode, and images were collected again.

2.7 Band Gap and Absorption Measurements

Band gap energies were measured by optical absorption spectroscopy, a previously established method for determining the band gap energies [33]. Each sample was placed in a 1 cm UV-Vis cuvette. If the sample was dark or opaque, it was diluted with the pH 8.5 Tris buffer solution until it was transparent but still retained its color. An arc xenon lamp was used as the broadband light source and run through a Digikrom spectrometer. The exiting light went through a mechanical chopper, which was used to reference a lock-in amplifier. The light then passed through the sample and was collected on a photodiode detector, which was connected to the signal input of the lock-in amplifier. The absorbance profile was built by running through a wide range of wavelengths. The resulting absorbance was used to calculate the band gap energies of each sample. A detailed explanation of the calculations can be found in work by Colton et al. [33].

Chapter 3

Results and Discussion

3.1 Manganese Nanoparticle Results

Manganese oxide nanoparticles were successfully synthesized within ferritin while using permanganate as the oxidant. The resulting core composition was noted to be dependent on pH and the specifics of this will be discussed below.

3.1.1 Evidence For Core Formation inside of Ferritin

All samples were synthesized according to methods outlined in the experimental section above. After synthesis, each sample was centrifuged and passed over our Sephadex G-100 gel filtration column to separate the unbound metals. In each case manganese was observed to migrate with ferritin as the samples were eluted from the column, as indicated by the retention of color and metals with the protein. The elution profile for the pH 5.4 permanganate only sample is displyed in Fig. 3.1 and is representative of all the elution profiles. Note how there are two main peaks in the profile: the first one represents the protein and its manganese core while the second one represents leftover manganese in solution. Ferritin with its metal core absorbs strongly in the lower end of the

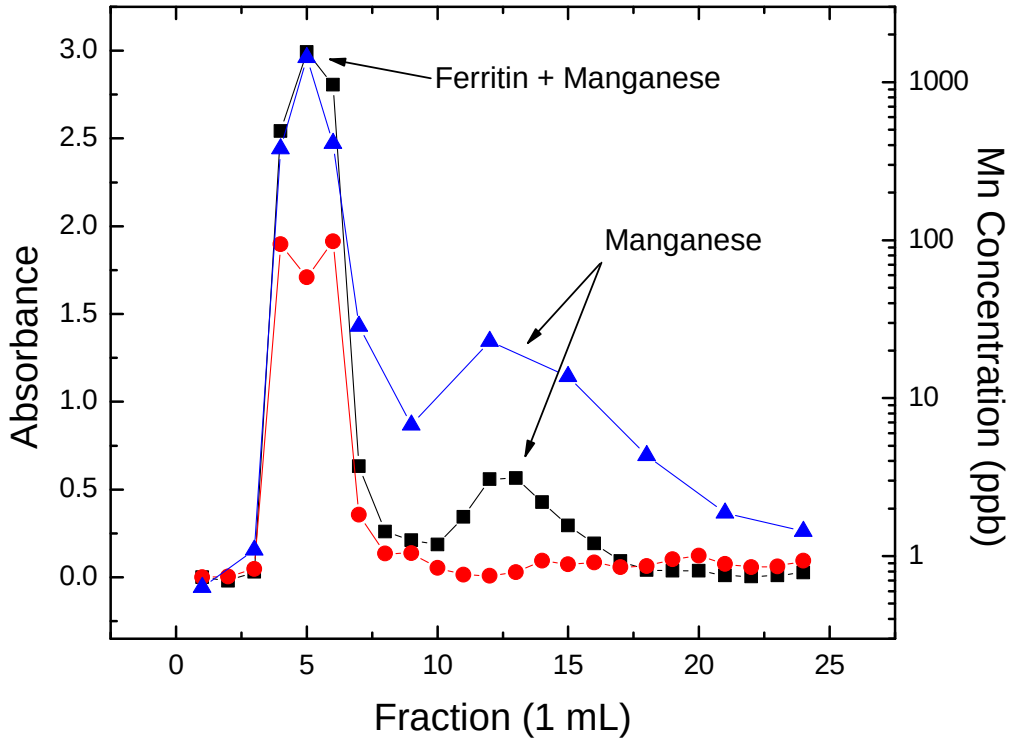

Figure 3.1 The elution profile for the pH 5.4 permanganate only sample. The absorbance is measured at 255 nm (black squares) and 420 nm (red circles). The concentration of manganese was measured by ICP-MS and is shown by the blue triangles.

visible spectrum and hence has strong absorbances at both 255 nm and 420 nm. Free manganese in solution, however, has a medium absorbance in the UV with little to no absorbance in the visible spectrum, as shown by the presence of 255 nm absorbance with virtually no 420 nm absorbance. Results from ICP-MS analysis are also shown in Fig. 3.1, providing further evidence for manganese associated with ferritin and separation from free manganese in solution.

After passing each sample over the column, most samples retained their color while some samples eluted clear, indicating apoferritin with no core formation.The comproportionation of Mn^{2+} and MnO_4^- with apoferritin at pH 5.4 and 9.4 successfully resulted in core formation for all ratios

(see Table 3.1). No significant core formation was observed for the comproportionation samples in the neutral buffer (pH 7.4), though high levels of precipitation were present. Control reactions without apoferritin present produced a dark-brown manganese precipitate and resulted in a clear solution after centrifugation; a similar precipitate was observed in all samples to a lesser extent, suggesting some manganese precipitation occurred outside of ferritin. The pH 9.4 samples all retained a medium-brown color even after centrifugation and filtration over the gel-exclusion column. The pH 5.4 samples also retained their color but were noticeably darker. The presence of color in the fractions containing ferritin after gel filtration indicates manganese core formation inside of ferritin.

Manganese cores were successfully synthesized using the comproportionation reactions under both aerobic and anaerobic conditions. The number of metals loaded per ferritin are reported in Table 3.1, as are the measured band gaps.

Table 3.1 also identifies the amount of protein lost during the reaction. Permanganate is a strong oxidizing species and is known to oxidize proteins. The fact that ferritin was not immediately oxidized and denatured in the presence of permanganate shows the remarkable stability of ferritin. One major difference noted between the aerobic and anaerobic samples was the amount of protein lost during the acidic reactions (see Table 3.1, samples 1–8). More protein was lost in the aerobic samples and for those with higher permanganate content. Additionally, the formation of manganese cores despite the absence of oxygen demonstrates permanganate's ability to act as the oxidant.

Adding only permanganate into the buffered apoferritin solution (i.e. no Mn^{2+} added) also resulted in core formation for both the acidic and basic conditions. A brown precipitate formed in each case, and was removed by centrifugation. The pH 5.4 buffered sample resulted in a dark-brown color once filtered over the gel-exclusion column, while the pH 9.4 sample resulted in a light brown-yellow color, indicative of lower amounts of manganese loading into the protein interior. The pH 7.4 sample resulted in core formation, but it was unstable and both the core and protein

Table 3.1 Results of both the permanganate only samples (samples 1, 5, 10, and 14) and the comproportionation samples (samples 2–4, 6–8, 11–13, and 14–17). Each section of data represents either the acidic or basic buffer solution run either aerobically or anaerobically. The listing of Traditional Method under the ratio of Mn:MnO_4^- column refers to the method originally discovered for manganese-ferritin synthesis using Mn^{2+} and oxygen. The band gap energies for samples 9 and 10 are left blank due to the core size being too small for band gap detection.

Sample	Ratio of Mn^{2+}:MnO_4^-	pH	Aerobic/ Anaerobic	Mn^{2+}/FTN Added	MnO_4^-/FTN Added	Final Mn/FTN	Protein (%) Loss	Indirect Band Gap (eV)	Direct Band Gap (eV)
1	0	5.4	Anaerobic	0	1500	716 ± 63	53	1.67 ± 0.02	2.68 ± 0.01
2	3:2	5.4	Anaerobic	900	600	629 ± 99	32	1.65 ± 0.02	2.64 ± 0.01
3	2:1	5.4	Anaerobic	1000	500	446 ± 63	27	1.65 ± 0.02	2.65 ± 0.02
4	4:1	5.4	Anaerobic	1200	300	265 ± 25	26	1.64 ± 0.02	265 ± 0.02
5	0	5.4	Aerobic	0	1500	580 ± 15	77	1.68 ± 0.02	2.70 ± 0.03
6	3:2	5.4	Aerobic	900	600	496 ± 19	57	1.65 ± 0.02	2.69 ± 0.01
7	2:1	5.4	Aerobic	1000	500	551 ± 62	39	1.63 ± 0.01	2.65 ± 0.02
8	4:1	5.4	Aerobic	1200	300	446 ± 55	30	1.64 ± 0.03	2.65 ± 0.02
9	Traditional Method	5.4	Aerobic	1500	0	51 ± 1	17	⋯	⋯
10	0	9.4	Anaerobic	0	1500	76 ± 6	32	⋯	⋯
11	3:2	9.4	Anaerobic	900	600	241 ± 20	18	1.58 ± 0.02	2.61 ± 0.02
12	2:1	9.4	Anaerobic	1000	500	406 ± 33	27	1.56 ± 0.01	2.62 ± 0.02
13	4:1	9.4	Anaerobic	1200	300	822 ± 112	27	1.58 ± 0.01	2.63 ± 0.01
14	0	9.4	Aerobic	0	1500	128 ± 10	29	1.80 ± 0.03	2.72 ± 0.02
15	3:2	9.4	Aerobic	900	600	152 ± 11	26	1.53 ± 0.02	2.59 ± 0.01
16	2:1	9.4	Aerobic	1000	500	148 ± 7	24	1.52 ± 0.03	2.66 ± 0.01
17	4:1	9.4	Aerobic	1200	300	283 ± 22	28	1.52 ± 0.02	2.65 ± 0.01
18	Traditional Method	9.4	Aerobic	1500	0	441 ± 25	9	1.53 ± 0.02	2.64 ± 0.03

precipitated after several hours. In the absence of ferritin, a brown precipitate likewise formed from the reactants and the solution was clear after removal of the precipitate by centrifugation.

Images taken with the TEM show the presence of nanoparticles inside ferritin. Representative bright field images for samples 3 and 12 from Table 1 are shown in Figs. 3.2(a) and 3.2(c). Other samples similarly showed core formation in ferritin. The metal cores are observed in the interior of ferritin as dark spots. The uranyl acetate stain was used to provide contrast for the protein shell,

and can be seen as the dark ring in the bright field images and the light ring in the STEM images [Figs. 3.2(b) and 3.2(d)].

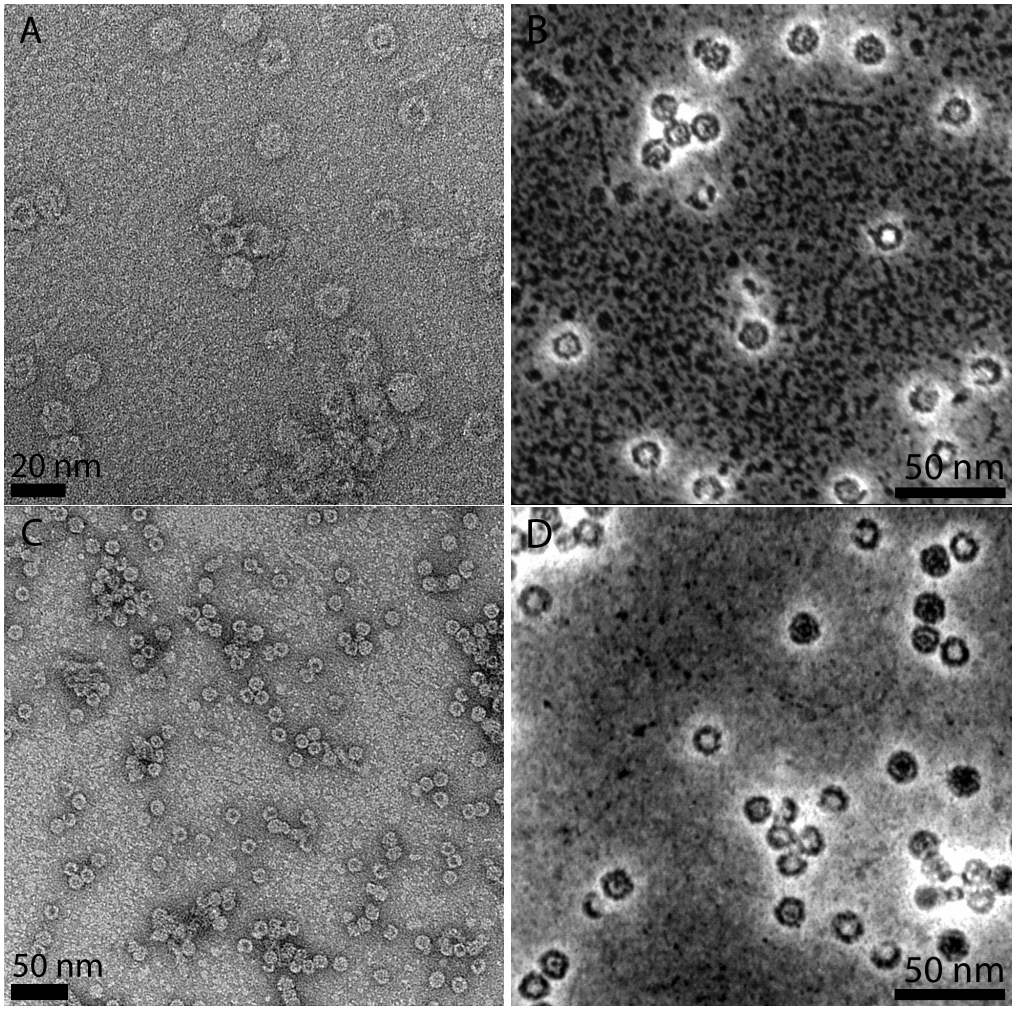

Figure 3.2 TEM analysis of stained manganese-loaded ferritin synthesized using a 2:1 ratio of Mn^{2+} and permanganate. (A) Bright field image of sample 3, run under anaerobic and acidic conditions. (B) STEM image of sample 3. (C) Bright field image of sample 12, run under anaerobic and basic conditions. (D) STEM image of sample 12.

3.1.2 Band Gap Meaurements of the Manganese Ferritin Minerals

Band gap measurements were performed on all of the samples via OAS to assist in determining whether a new manganese core had formed. The manganese minerals formed by the above methods were found to be indirect band gap semiconductors, which was also observed in the Mn(O)OH ferritin minerals studied by Erickson et al. [34]. The band gaps for each of these samples are listed in Table 3.1. Our manganese-ferritin samples were measured to have indirect gaps up to 0.27 eV higher than the traditional manganese ferritin, with slight changes (less than 0.1 eV in either direction) for the direct transition. We attribute these changes in the band gap energies to the formation of a new manganese core inside some of the ferritin samples.

It is interesting to note that the anaerobic basic samples have a slightly higher indirect band gap energy than their aerobic counterparts (as little as 0.03 and up to 0.06 eV higher). Since the aerobic samples (samples 15–17) have smaller cores than the corresponding anaerobic samples (samples 11–13), our samples show the opposite trend that one would expect to occur due to quantum confinement (where smaller cores have larger band gaps). For example, sample 17 has approximately 283 manganese/ferritin with an indirect band gap of 1.52 eV, while sample 13 (the same ratio and pH but performed anaerobically) has an average core size of 822 manganese/ferritin with an indirect band gap of 1.58 eV. This discrepancy suggests that the cores formed in the anaerobic trials may have a slightly different composition than their aerobic counterparts. We also note that the basic conditions gave us band gap energies similar to the traditional sample, while the acidic samples had indirect band gap energies up to 0.16 eV higher.

3.1.3 Discussion of Permanganate Only Reactions

As stated above, manganese was observed to load into ferritin in the permanganate only samples, where no Mn^{2+} was present. Significantly more metals were loaded in the acidic condition (see Table 1, comparing samples 1 and 5 with 10 and 14). In the acidic buffer solution, the presence

of oxygen increased the protein loss from 53% to 77%, while simultaneously decreasing the total number of metals loaded from 716 Mn/ferritin to 580 Mn/ferritin. We observed that the acidity of the solution greatly affected the manganese incorporation into ferritin. This dependence on the pH of the solution follows the self-reduction mechanism of permanganate while in the presence of acid [26, 38], as shown in the following equation:

$$4\,MnO_4^- + 4\,H^+ \rightarrow 4\,MnO_2 + 3\,O_2 + 2\,H_2O. \tag{3.1}$$

Equation 3.1 also agrees with the observation that the presence of oxygen inhibits the self-reduction of permanganate under acidic conditions, requiring it to use the protein as a source of electrons instead (compare samples 1 and 5, where 1 has higher metals/ferritin and less protein loss). The dependence on pH as well as the effect of oxygen on the reaction likewise suggests the formation of MnO_2 inside ferritin. Under these circumstances, permanganate likely migrates into the ferritin interior before interacting with ferritin and producing a manganese oxide, though some precipitation would likely still occur outside of ferritin as well.

The absorption profiles of these permanganate only samples, shown in Fig. 3.3, also suggest some amount of MnO_2 formation. The increased absorption near 370 nm has previously been identified as a characteristic of MnO_2 formed by reducing permanganate [26] and suggests MnO_2 formation in our ferritin samples. Note how this increased absorption is absent in the traditional Mn(O)OH-ferritin, giving evidence to the formation of a new manganese mineral in ferritin. The overall absorption of the samples also increases due to the increase in manganese ions per ferritin.

Lastly, we note that the indirect band gap for sample 10 is significantly higher than all other samples run at pH 9.4. Sample 10 was also noted to have a slight amount of the characteristic 370 nm absorption, which may be part of the reason for a higher band gap energy. Due to the small core size (128 Mn/ferritin), sample 10 may also be approaching the size at which it no longer has any detectable band gap energy (compare to samples 9 and 10 which had undetectable band gaps and 51 and 76 Mn/ferritin, respectively), which smaller size contributes to the higher indirect band

gap energy because of quantum confinement.

The results from the permanganate only reactions show how much manganese loads into ferritin due to the interaction between ferritin and permanganate. Comparing the number of metals loaded in the anaerobic comproportionation (samples 11–13) and permanganate only reactions (sample 10) at pH 9.4 shows that very little of the manganese loaded during the comproportionation reactions can be attributed to permanganate only. For example, sample 10 had an average of 72 Mn/ferritin, as compared to sample 13, which loaded 822 Mn/ferritin. Thus, a maximum of 72 Mn/ferritin can be attributed to the permanganate reacting with apoferritin by itself. Additionally, since permanganate reacts with Mn^{2+} and forms a precipitate in solution, less permanganate will be available for direct incorporation into ferritin. Hence, permanganate will contribute very few metals to the core formed during the basic reactions due to self-reduction (i.e. the reaction in Eq. 3.1), and the vast majority of manganese comes from the reaction of permanganate with Mn^{2+}. For the anaerobic acidic trial, it seems likely that a significant amount of the manganese incorporated into ferritin comes from the self-reduction of permanganate, as 716 manganese atoms loaded per ferritin in the permanganate only sample.

3.1.4 Discussion of Comproportionation Reactions

As mentioned previously, the reaction of permanganate and Mn^{2+} in the presence of apoferritin resulted in the formation of a manganese mineral inside of ferritin. Manganese loading occurred in all anaerobic samples, despite the absence of oxygen. In sample 13, an anaerobic trial, more manganese loaded per ferritin than possible due to permanganate alone (822 Mn atoms were loaded with a maximum of 300 being from permanganate), meaning that some amount of Mn^{2+} was oxidized by permanganate and incorporated into the core. This demonstrates permanganate's ability to act as the oxidant in the absence of oxygen.

In each trial, up to half of the total metals deposited themselves into ferritin, as shown in Table

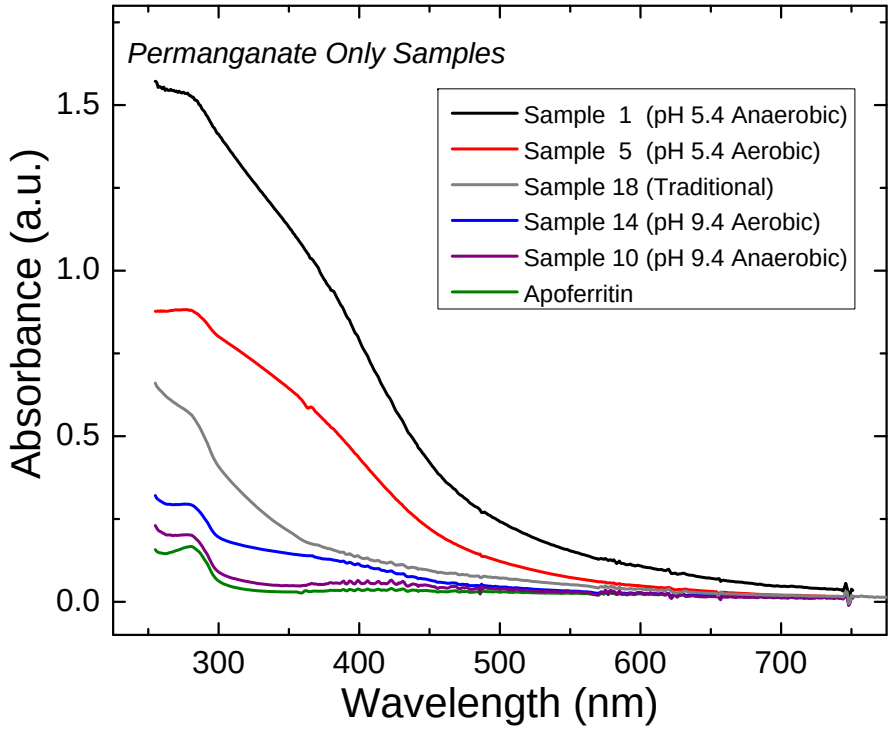

Figure 3.3 The absorption spectra of manganese-loaded ferritin synthesized using permanganate only. Each sample was prepared at 0.10 mg/mL ferritin, and the traditional manganese-ferritin and apoferritin are included for comparison. The legend follows the samples from top to bottom. Note how samples 1, 5, and 14 have an increased absorption shoulder near 370 nm, indicative of a new mineral formation.

1. The loss of metal is due to the precipitation that occurred outside of ferritin, which precipitate was removed from the solution during centrifugation. As mentioned previously, this precipitate resulted from Mn^{2+} and permanganate reacting before Mn^{2+} diffusion into and interaction with ferritin.

X-ray diffraction (XRD) and electron diffraction were both used in an attempt to characterize the mineral and to determine which proposed mechanism the reactions follow. Results showed the presence of an amorphous manganese core in each case, making it impossible to determine the mineral type through these methods. This result is not entirely unexpected as ferritin often forms amorphous cores in its interior [18].

We also measured the absorption profiles for each of the comproportionation samples to help differentiate our new manganese ferritin from the traditionally synthesized manganese-ferritin (sample 18). The spectra of samples 2 and 13 are plotted alongside the traditional manganese-ferritin sample in Figure 7, and all samples were prepared at 0.1 mg/ml ferritin. All acidic samples had absorption profiles similar to the sample 2 as shown in Fig. 3.4, and the basic samples were similar to the one selected for the same figure (sample 13). The presence of oxygen had no apparent effect on the absorption profiles other than to change the strength of the absorption by changing the number of metals loaded. These samples were chosen because they had the highest metal loading in the basic and acidic groups and helped highlight the differences between these two groups.

In the absorption profiles for these samples, part of the absorption at 280 nm comes from the protein itself, while the absorption tailing into the visible wavelengths arises solely from the metal-oxide cores. An increase in absorption near 370 nm appears in the profiles of the acidic comproportionation samples, a trait which is absent in both the basic samples and the traditional sample but present in the permanganate only reactions. This increased absorption confirms the presence of a new mineral within ferritin. As discussed in the permanganate only section, this increase in absorption near 370 nm has been observed with the formation of MnO_2 and suggests

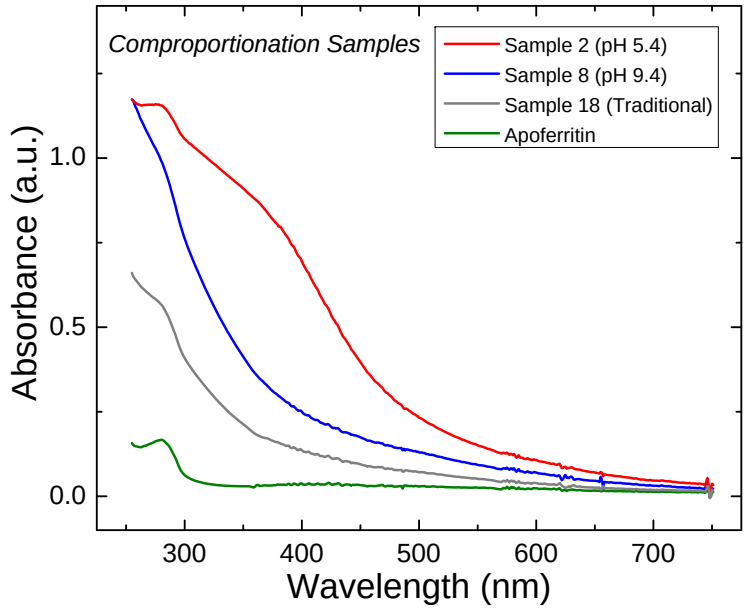

Figure 3.4 The absorption spectra of manganese-loaded ferritin samples, synthesized by comproportionation of Mn^{2+} and MnO_4^-. From top to bottom the samples are: red curve, 3:2 ratio of Mn^{2+} to MnO_4^- at pH 5.4; blue curve, 4:1 ratio at pH 9.4; gray curve, sample prepared through the traditional method at pH 9.4; and green curve, apoferritin.

the formation of MnO_2 within our ferritin. The formation of MnO_2 in these samples indicates that the reactions outlined in Eqs. 1.4 and 3.1 occur to produce this sample.

The basic samples, on the other hand, appear quite similar to the traditional sample, and suggest the Mn(O)OH mineral formed through a similar reaction mechanism. This result suggests that the basic conditions make use of the ferroxidase center, as outlined in Eqs. (1) and (2). In the aerobic trials, permanganate competes with oxygen and is less able to assist in loading at the ferroxidase center. Hence it is left to react with Mn^{2+} in solution, and fewer metals are available to load into ferritin. This effect is seen by comparing the total metal loading in the anaerobic and aerobic samples synthesized under basic conditions (compare samples 11–13 with samples 15–17). However, in the absence of oxygen, permanganate is allowed to oxidize Mn^{2+} at the

ferroxidase center rather than precipitating in solution, nearly doubling the total number of metals loaded. Permanganate acting at the ferroxidase center could lead to higher incorporation of reduced permanganate into the ferritin core, possibly explaining the slight increases we observed in band gap energies between the aerobic and anaerobic samples at pH 9.4. Despite these possibilities, however, it is difficult to determine which reaction occurs in each condition because of protein loss and the amorphous nature of the mineral.

We also noted that the samples with an increased 370 nm absorption correlated with an increase in the indirect band gap energies. The acidic samples (samples 1–8) all have indirect band gaps near 1.65 eV, while all basic samples (samples 11–18) have indirect band gap energies similar to the traditional manganese sample close to 1.53 eV. We note our traditional sample has a band gap energies slightly below those reported by [34], which may be a consequence of the different pH buffer used to separate the protein over the gel-exclusion column. The similarities in absorbance and band gap energies between the basic samples and the traditional manganese sample strengthen our conclusion that a similar mineral formed in each case by a similar mechanism. The differences noted between the acidic and basic samples gives evidence to a new mineral formation in the acidic conditions.

3.2 Cobalt-Manganese Nanoparticle Results

3.2.1 Evidence For Core Formation inside of Ferritin

All samples were centrifuged at 3100 $\times$ *g* for 10 minutes and we observed small amount of precipitate at the bottom of our solution. We then passed each sample over a Sephadex G-100 filtration column (12.5 cm $\times$ 1 cm) to separate the ferritin from unbound manganese and cobalt metals. In the cases where a metal oxide core formed inside of ferritin, some metals migrated over the column with the ferritin while others remained behind in solution. An elution profile for sample 6 is shown

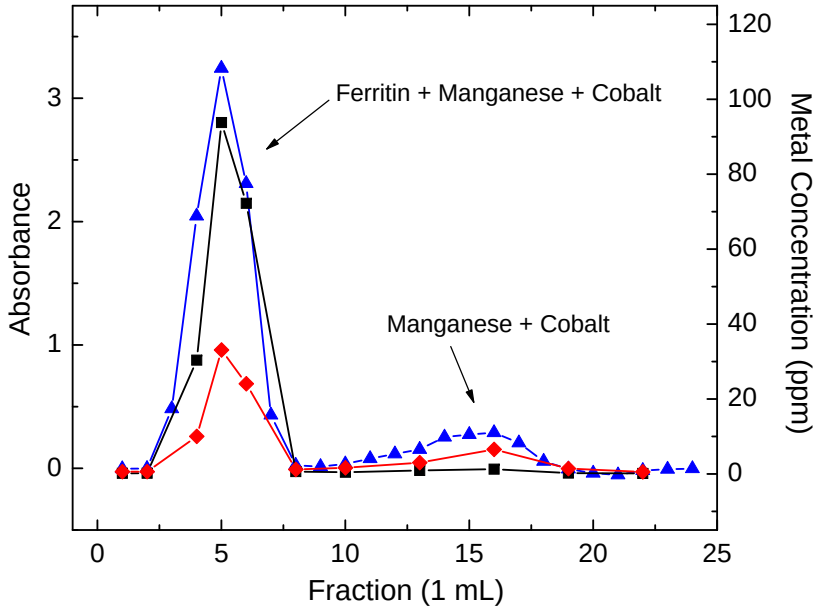

Figure 3.5 The elution profile for the sample 6. The absorbance is measured at 320 nm (blue triangles). The concentration of manganese and cobalt were measured by ICP-MS and are shown by the black squares and red diamonds, respectively.

in Figure 3.5 and shows the separation of unbound metals from the ferritin protein. The metals in each fraction eluted from the column were determined by ICP-MS to demonstrate how each metal separated, and the absorption was measured at 320 nm for each fraction. Free salt also absorbs stronly in the UV, and accounts for the second absorption peak on the right side of the graph. Cobalt and manganese were both observed to elute from the column with ferritin, as demonstrated by the two peaks, the first one being the protein with its mineral core. From the second peak, we can see that more cobalt is present in the second peak for this sample, indicating leftover cobalt metals from the reaction. Meanwhile, free manganese levels were very low in solution, likely due to high levels of manganese incorporation into ferritin as well as some precipitation that occurred outside of ferritin.

Mixed cobalt-manganese samples were formed in almost every reaction, and the average num-

Table 3.2 Table of the cobalt-manganese samples synthesized at pH 8.5. Samples 1 and 2 had core sizes too small to allow for detection of their band gap energies.

Sample	Co^{2+}/FTN Added	MnO_4^-/FTN Added	Final Co/FTN	Final Mn/FTN	Final Metal/FTN	Relative Protein Loss (%)	Indirect Band Gap (eV)	Direct Band Gap (eV)
1	1600	0	28 ± 2	0 ± 0	28 ± 2	0	···	···
2	1400	200	50 ± 5	41 ± 4	91 ± 9	4	···	···
3	1200	400	71 ± 3	111 ± 5	182 ± 8	5	1.53 ± 0.02	3.04 ± 0.05
4	1000	600	129 ± 10	285 ± 23	414 ± 34	8	1.48 ± 0.02	2.82 ± 0.03
5	800	800	214 ± 25	568 ± 66	782 ± 90	7	1.49 ± 0.02	2.80 ± 0.02
6	600	1000	264 ± 48	838 ± 151	1102 ± 199	9	1.50 ± 0.02	2.78 ± 0.01
7	400	1200	193 ± 25	899 ± 115	1092 ± 140	23	1.57 ± 0.01	2.78 ± 0.04
8	200	1400	92 ± 9	936 ± 95	1028 ± 95	35	1.65 ± 0.01	2.73 ± 0.01
9	0	1600	0 ± 0	538 ± 99	538 ± 99	33	1.75 ± 0.03	2.73 ± 0.01

ber of metals loaded into ferritin is shown in Table 3.2, as are the relative loss of protein and the band gap energies. Samples eluted over the column retained a medium brown color with a hint of olive green.

The average number of metals per ferritin was calculated using the protein and metal concentrations of each of our samples. The number of manganese atoms, cobalt atoms, and total metal atoms per ferritin are shown in Table 3.2.

Images taken on the TEM are shown below in Fig. 3.6. The protein shell is the dark circle with the light halo around it, which comes from the uranyl acetate stain. The metal oxide core is shown by the bright core inside the protein shell. These images, combined with the elemental information obtained by the ICP-MS, confirms the formation of a metal oxide core inside of ferritin.

3.2.2 Band Gap Meaurements of the Manganese Ferritin Minerals

Band gap measurements were performed on all samples by OAS, and measurable band gaps were detected for samples 3–9. It was determined that each of these samples behave as indirect band gap materials with a direct transition, similar to nanoparticles previously formed within ferritin [33,34].

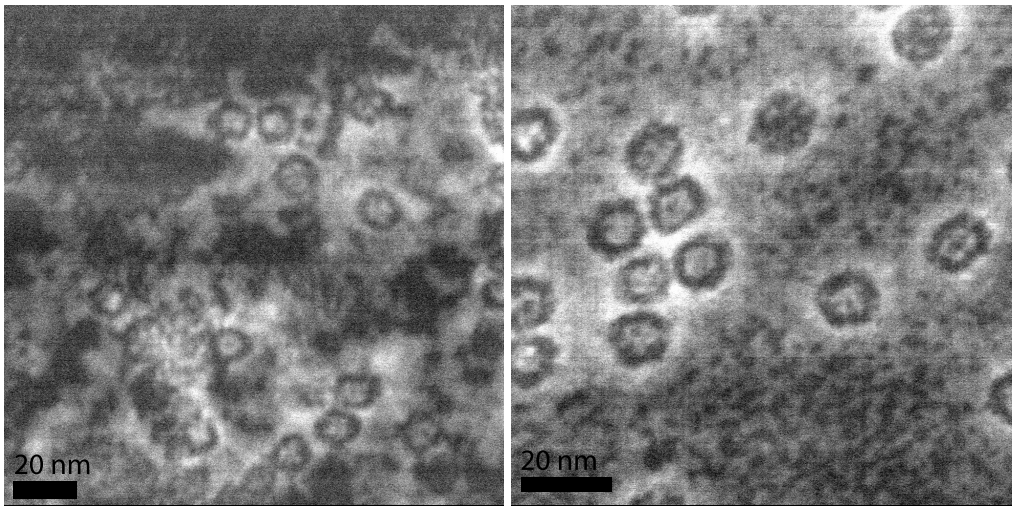

Figure 3.6 (a) STEM image of cobalt-manganese ferritin (sample 6). (b) STEM image of sample 4.

Samples 1 and 2 showed no detectable band gap energies. The band gap energy measurements for the samples are included in Table 3.2 and the energies are plotted versus the sample number in Fig. 3.7.

As the relative amount of manganese in each sample increased, the indirect band gap energies increased while the direct band gap energies decreased. The sample synthesized using entirely permanganate (sample 9) showed an indirect band gap energy of 1.75 eV; and as the amount of cobalt was increased, the indirect band gap energy decreased until the lowest energy was detected for sample 4 at 1.48 eV. The direct gaps showed a reverse trend, with band gap energies ranging from 2.73 eV up to 3.04 eV.

3.2.3 Discussion of Results

The reaction of Co^{2+} and MnO_4^- resulted in the formation of a mixed metal core within ferritin. We obtained the average number of metals loaded per ferritin through use of an ICP-MS, and we observed that the number of metals loaded per ferritin varied widely from essentially no metals

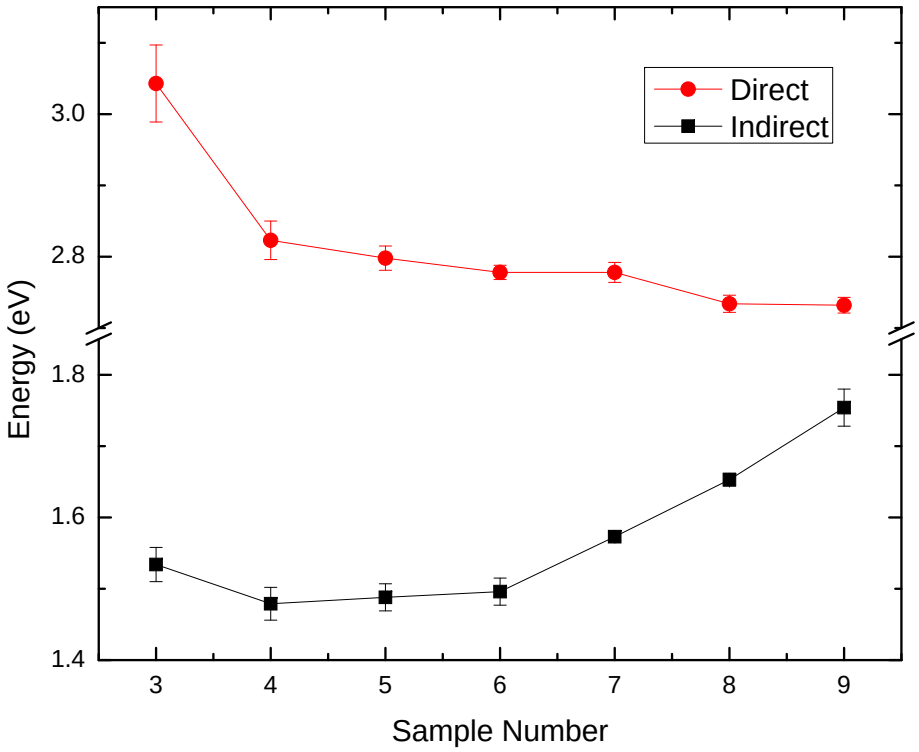

Figure 3.7 A graph of the band gap energies for samples 3–9. The energies are plotted versus the sample number to which each band gap energy belongs. The sample numbers also relate the to amount of manganese compared to cobalt in the final ferritin mineral, and an increasing sample number corresponds to increasing the amount of manganese relative to cobalt in the sample. Core sizes were too small for detectable band gap energies in samples 1 and 2.

(see sample 1) to almost 75% of our target loading (see sample 6). Metal loading less than the targeted amount of 1600 occurred for each sample. We noted previously that some precipitation had occured, a likely result of the reaction between Co^{2+} and MnO_4^- occurring outside of solution. Additionally, the elution profile for sample 6 (Fig. 3.5) showed that a small amount of unreacted cobalt remained in solution, as indicated by the large concentration that eluted out in fractions 14–20.

The amount of protein lost during the reaction increased as the amount of permanganate added was increased and the amount of cobalt was decreased. The loss of the electron donor (Co^{2+}) and

an increase in our oxidizing agent (MnO_4^-) led to more permanganate, which was forced to turn to the protein to find electrons. This caused the protein denaturation and caused it to precipitate out of solution. When the ratio of permanganate to cobalt exceeded 1.67, the amount of protein loss began to increase dramatically and the efficiency of manganese loading decreased (see samples 7–9). We also noted that the number of manganese loaded into ferritin in sample 9 (0 cobalt added per ferritin) was almost half of that of sample 8, where 200 cobalt atoms were added per ferritin. This small increase in cobalt allowed for a much greater incorporation of manganese into ferritin, showing how cobalt also assists manganese loading into ferritin.

Samples with little to no permanganate present showed minimal loading into ferritin (samples 1 and 2), where less than 100 metals loaded per ferritin. This demonstrates permanganate's role as the oxidizing agent and that it is necessary to allow for cobalt incorporation into the core. During or after the reaction between permanganate and cobalt, manganese is also incorporated into the ferritin mineral, as detected by ICP-MS analysis. Both manganese and cobalt loaded most efficiently in sample 6, which had the highest total amount of metals loaded while losing less than 10% of total protein when compared to sample 1. Efficient loading of cobalt and manganese into ferritin thus requires both metals to be present, with an optimal ratio near 1.67 between manganese and cobalt (sample 6).

The ratio of cobalt and permanganate also greatly affected the band gap energies of the samples. The indirect band gap energies showed a positive trend with increasing manganese content. Sample 9, synthesized using entirely permanganate, had the highest indirect band gap energy at 1.75 eV. As cobalt was added, the band gap energy dropped dramatically, but slowed down in its decent as more and more cobalt were added. Sample 3 appears to be somewhat of an anomaly as its band gap energy actually increased upon increasing cobalt relative to manganese. This may be the effect of the mineral size and quantum confinement (where smaller nanoparticles experience increased band gap energies), as sample 3 has a much smaller mineral size as compared to the other samples

with less than 200 metals per ferritin. The direct band gap energies show the reverse trend, with energies increasing as the relative amount of cobalt increases. Thse trends are shown above in Fig. 3.7.

Chapter 4

Conclusions

4.1 Permanganate as the Oxidant for Nanoparticle Synthesis

We have discovered a new synthesis method for preparing manganese minerals inside ferritin by reacting permanganate and Mn^{2+} in the presence of apoferritin. In the absence of oxygen, permanganate acts as the oxidant and is able to oxidize Mn^{2+} to form the manganese oxide core. Manganese loading into ferritin was established by ICP-MS and TEM imaging. This reaction performed in an acidic environment leads to the formation of a new manganese oxide core inside ferritin. Differences between the traditional samples and those synthesized in an acidic environment include changes in the indirect band gap energies by up to 0.16 eV and significant changes in the absorption profile. These differences suggest that the comproportionation of Mn^{2+} and permanganate in an acidic solution form a MnO_2 core inside ferritin (having a +4 oxidation state), as opposed to the Mn(O)OH core that forms in the basic solution and the traditional samples (a +3 state). By changing the pH of the buffered solution, we are able to alter the mineral formed, thus changing the band gap energies and increasing ferritin's ability to act as a photosensitive substrate.

Additionally, we have successfully synthesized a cobalt-manganese mixed metal core within

ferritin by reacting permanganate and Co^{2+} in the presence of apoferritin. Cobalt and manganese loading were established by ICP-MS and TEM imaging. The band gap energies of these samples were shown to be highly dependent upon the ratio of Co and Mn loaded into ferritin.

4.2 Directions for Future Work

The goal of this project is to develop ferritin-based solar cells. Erickson et al. demonstrated that efficiencies of these cells could be greatly increased by finding a substrate with a band gap energy near that of silicon [34]. We have planned to synthesize and characterize PbS nanoparticles within ferritin and measure the size-dependence of their band gap energies (see work done by Hennequin et al.) [16]. Once we have gathered these materials, we will incoroporate them into dye-sensitized solar cells and determine their efficiency of solar energy conversion.

Bibliography

[1] N. D. Chasteen, B. C. Antanaitis, and P. Aisen, "Iron Deposition in Apoferritin," J. Biol. Chem. **260,** 2926–2929 (1985).

[2] E. C. Theil, "Ferritin: Structure, Gene Regulation, and Cellular Function in Animals, Plants, and Microorganisms," Annual Review of Biochemistry **56,** 289–315 (1987), pMID: 3304136.

[3] N. Chasteen and P. M. Harrison, "Mineralization in Ferritin: An Efficient Means of Iron Storage," Journal of Structural Biology **126,** 182 – 194 (1999).

[4] P. M. Harrison and P. Arosio, "The ferritins: molecular properties, iron storage function and cellular regulation," Biochimica et Biophysica Acta (BBA) - Bioenergetics **1275,** 161 – 203 (1996).

[5] M. Kim, Y. Rho, K. S. Jin, B. Ahn, S. Jung, H. Kim, and M. Ree, "pH-Dependent Structures of Ferritin and Apoferritin in Solution: Disassembly and Reassembly," Biomacromolecules **12,** 1629–1640 (2011), pMID: 21446722.

[6] F. C. Meldrum, V. J. Wade, D. L. Nimmo, B. R. Heywood, and S. Mann, "Synthesis of inorganic nanophase materials in supramolecular protein cages," Nature **349,** 684 – 687 (1991).

[7] T. Douglas and V. T. Stark, "Nanophase Cobalt Oxyhydroxide Mineral Synthesized within the Protein Cage of Ferritin," Inorganic Chemistry **39,** 1828–1830 (2000).

[8] I. Urushizaki, Y. Niitsu, K. Ishitani, M. Matsuda, and M. Fukuda, "Microheterogeneity of horse spleen ferritin and apoferritin," Biochimica et Biophysica Acta (BBA) - Protein Structure **243,** 187 – 192 (1971).

[9] X. Peng and I. Ichinose, "Flexible free-standing ultrathin or thin protein membrane, its fabrication method and application,", 2014, U.S. Patent 8,828,239.

[10] A. Mazur, I. Litt, and E. Shorr, "CHEMICAL PROPERTIES OF FERRITIN AND THEIR RELATION TO ITS VASODEPRESSOR ACTIVITY," Journal of Biological Chemistry **187,** 473–484 (1950).

[11] J. Polanams, A. D. Ray, , and R. K. Watt*, "Nanophase Iron Phosphate, Iron Arsenate, Iron Vanadate, and Iron Molybdate Minerals Synthesized within the Protein Cage of Ferritin," Inorganic Chemistry **44,** 3203–3209 (2005), pMID: 15847428.

[12] J. L. Johnson, M. Cannon, R. K. Watt, R. B. Frankel, , and G. D. Watt, "Forming the Phosphate Layer in Reconstituted Horse Spleen Ferritin and the Role of Phosphate in Promoting Core Surface Redox Reactions," Biochemistry **38,** 6706–6713 (1999), pMID: 10350490.

[13] H. Huang, R. K. Watt, R. B. Frankel, and G. D. Watt, "Role of phosphate in iron(2+) binding to horse spleen holoferritin," Biochemistry **32,** 1681–1687 (1993), pMID: 8431449.

[14] A. Trefry and P. M. Harrison, "Incorporation and release of inorganic phosphate in horse spleen ferritin," Biochemical Journal **171,** 313–320 (1978).

[15] T. J. Smith, S. D. Erickson, C. M. Orozco, A. Fluckiger, L. M. Moses, J. S. Colton, and R. K. Watt, "Tuning the band gap of ferritin nanoparticles by co-depositing iron with halides or oxo-anions," J. Mater. Chem. A **2,** 20782–20788 (2014).

[16] B. Hennequin, L. Turyanska, T. Ben, A. M. Beltran, S. I. Molina, M. Li, S. Mann, A. Patane, and N. R. Thomas, "Aqueous Near-Infrared Fluorescent Composites Based on Apoferritin-Encapsulated PbS Quantum Dots," Advanced Materials **20,** 3592–3596 (2008).

[17] H.-A. Hosein, D. R. Strongin, M. Allen, and T. Douglas, "Iron and Cobalt Oxide and Metallic Nanoparticles Prepared from Ferritin," Langmuir **20,** 10283–10287 (2004), pMID: 15518526.

[18] P. Mackle, J. M. Charnock, C. D. Garner, F. C. Meldrum, and S. Mann, "Characterization of the manganese core of reconstituted ferritin by x-ray absorption spectroscopy," Journal of the American Chemical Society **115,** 8471–8472 (1993).

[19] M. T. Klem, J. Mosolf, M. Young, and T. Douglas, "Photochemical Mineralization of Europium, Titanium, and Iron Oxyhydroxide Nanoparticles in the Ferritin Protein Cage," Inorganic Chemistry **47,** 2237–2239 (2008), pMID: 18307300.

[20] T. Douglas, D. P. E. Dickson, S. Betteridge, J. Charnock, and e. al, "Synthesis and structure of an iron(III) sulfide-ferritin bioinorganic nanocomposite," Science **269,** 54 (1995), copyright - Copyright American Association for the Advancement of Science Jul 7, 1995; Last updated - 2010-06-08; CODEN - SCIEAS.

[21] K. K. W. Wong and S. Mann, "Biomimetic synthesis of cadmium sulfide-ferritin nanocomposites," Advanced Materials **8,** 928–932 (1996).

[22] C. A. Butts, J. Swift, S. gu Kang, L. D. Costanzo, D. W. Christianson, J. G. Saven, and I. J. Dmochowski, "Directing Noble Metal Ion Chemistry within a Designed Ferritin Protein,," Biochemistry **47,** 12729–12739 (2008), pMID: 18991401.

[23] D. Ensign, M. Young, and T. Douglas, "Photocatalytic Synthesis of Copper Colloids from Cu(II) by the Ferrihydrite Core of Ferritin," Inorganic Chemistry **43,** 3441–3446 (2004), pMID: 15154806.

[24] F. C. Meldrum, T. Douglas, S. Levi, P. Arosio, and S. Mann, "Reconstitution of manganese oxide cores in horse spleen and recombinant ferritins," Journal of Inorganic Biochemistry **58,** 59 – 68 (1995).

[25] K. Pisarczyk and U. by Staff, in *Kirk-Othmer Encyclopedia of Chemical Technology* (John Wiley and Sons, Inc., 2000).

[26] T. Fujimoto, Y. Mizukoshi, Y. Nagata, Y. Maeda, and R. Oshima, "Sonolytical preparation of various types of metal nanoparticles in aqueous solution," Scripta Materialia **44,** 2183 – 2186 (2001).

[27] B. Zhang, J. N. Harb, R. C. Davis, J.-W. Kim, S.-H. Ch, S. Choi, T. Miller, , and G. D. Watt, "Kinetic and Thermodynamic Characterization of the Cobalt and Manganese Oxyhydroxide Cores Formed in Horse Spleen Ferritin," Inorganic Chemistry **44,** 3738–3745 (2005), pMID: 15877458.

[28] E. C. Theil, "Ferritin: At the Crossroads of Iron and Oxygen Metabolism," The Journal of Nutrition **133,** 1549S–1553S (2003).

[29] D. J. Price and J. G. Joshi, "Ferritin: Protection of enzymatic activity against the inhibition by divalent metal ions in vitro," Toxicology **31,** 151 – 163 (1984).

[30] D. Price and J. G. Joshi, "Ferritin: A zinc detoxicant and a zinc ion donor," Proceedings of the National Academy of Science **79,** 3116–3119 (1982).

[31] D. L. Jacobs, G. D. Watt, R. B. Frankel, and G. C. Papaefthymiou, "Redox reactions associated with iron release from mammalian ferritin," Biochemistry **28,** 1650–1655 (1989).

[32] D. Hopwood, "Fixation of proteins by osmium tetroxide potassium dichromate and potassium permanganate," Histochemie **18,** 250–260 (1969).

[33] J. S. Colton, S. D. Erickson, T. J. Smith, and R. K. Watt, "Sensitive detection of surface- and size-dependent direct and indirect band gap transitions in ferritin," Nanotechnology **25,** 135703 (2014).

[34] S. D. Erickson, T. J. Smith, L. M. Moses, R. K. Watt, and J. S. Colton, "Non-native Co-, Mn-, and Ti-oxyhydroxide nanocrystals in ferritin for high efficiency solar energy conversion," Nanotechnology **26,** 015703 (2015).

[35] O. H. Lowry, N. J. Rosebrough, A. L. Farr, and R. J. Randall, "PROTEIN MEASUREMENT WITH THE FOLIN PHENOL REAGENT," Journal of Biological Chemistry **193,** 265–275 (1951).

[36] M. M. Bradford, "A rapid and sensitive method for the quantitation of microgram quantities of protein utilizing the principle of protein-dye binding," Analytical Biochemistry **72,** 248 – 254 (1976).

[37] B.-G. Han, R. W. Walton, A. Song, P. Hwu, M. T. Stubbs, S. M. Yannone, P. ArbelÃąez, M. Dong, and R. M. Glaeser, "Electron microscopy of biotinylated protein complexes bound to streptavidin monolayer crystals," Journal of Structural Biology **180,** 249 – 253 (2012).

[38] A. H. Webster and J. Halpern, "Kinetics of the reduction of permanganate in aqueous solution by molecular hydrogen," Trans. Faraday Soc. **53,** 51–60 (1957).

Index